Available online at www.sciencedirect.com

ScienceDirect

journal homepage: www.elsevier.com/locate/he

Assessment of power and hydrogen production performance of an integrated system based on middle-grade geothermal source and solar energy

Ayhan Atiz [a], *Hatice Karakilcik* [b], *Mustafa Erden* [c], *Mehmet Karakilcik* [c,*]

[a] *Department of Mathematics and Science Education, Faculty of Education, Alanya Alaaddin Keykubat University, 07400, Antalya, Turkey*

[b] *Department of Geology Engineering, Faculty of Engineering, Cukurova University, 01250, Adana, Turkey*

[c] *Department of Physics, Faculty of Sciences and Letters, Cukurova University, 01250, Adana, Turkey*

HIGHLIGHTS

- A comprehensive study on performance of an integrated system working with various working fluids.
- Upgraded of the middle-grade geothermal resource temperature by use solar energy via PTSCs.
- The working fluid mass flow rate plays a key role of system on thermal performance.
- Exergetic performance of cyclohexane decreases sharply in temperature drops.
- n-butane is quite effect on the electricity and hydrogen generation performance of the system.

GRAPHICAL ABSTRACT

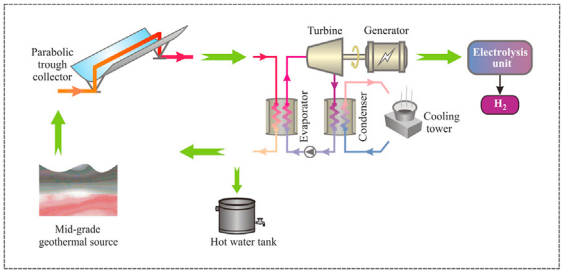

ARTICLE INFO

Article history:
Received 6 August 2020
Received in revised form
2 October 2020
Accepted 3 October 2020
Available online 29 October 2020

Keywords:
Middle-grade geothermal source
Parabolic trough solar collectors
Organic rankine cycle

ABSTRACT

In this study, power and hydrogen production performance of an integrated system is investigated. The system consists of an organic Rankine cycle (ORC), parabolic trough solar collectors (PTSCs) having a surface area of 545 m^2, middle-grade geothermal source (MGGS), cooling tower and proton exchange membrane (PEM). The final product of this system is hydrogen that produced via PEM. For this purpose, the fluid temperature of the geothermal source is upgraded by the solar collectors to drive the ORC. To improve the electricity generation efficiency, four working fluids namely n-butane, n-pentane, n-hexane, and cyclohexane are tried in the ORC. The mass flow rate of each working fluid is set as 0.1, 0.2, 0.3, 0.4 kg/s and calculations are made for 16 different situations (four types of working fluids and four different mass flow rates for each). As a result, n-butane with a mass flow rate of 0.4 kg/s is found to be the best option. The average electricity generation

* *Corresponding author.*
E-mail address: kkilcik@cu.edu.tr (M. Karakilcik).

https://doi.org/10.1016/j.ijhydene.2020.10.016

0360-3199/© 2020 Hydrogen Energy Publications LLC. Published by Elsevier Ltd. All rights reserved.

Power generation
Hydrogen production

is 66.02 kW between the hours of 11^{00}-13^{00}. The total hydrogen production is 9807.1 g for a day. The energy and exergy efficiency is calculated to be 5.85% and 8.27%, respectively.

© 2020 Hydrogen Energy Publications LLC. Published by Elsevier Ltd. All rights reserved.

Nomenclature

A	aperture area (m^2)
C	specific heat
$\dot{E}$	energy (W or kW)
$\dot{E}x$	exergy (W or kW)
ex	specific exergy (kJ/kg)
h	enthalpy (kJ/kg)
$\dot{I}$	solar radiation (W/m^2)
$\dot{m}$	mass flow rate (kg/s)
$\dot{Q}$	heat (kW)
T	temperature (°C or K)
$\dot{W}$	power (kW)

Greek symbols

η	energy efficiency
ψ	exergy efficiency

Subscripts

bp	beam parabolic
con	condenser
comp	compressor
PTSCs	parabolic through solar collectors
eva	evaporator
G	generator
GEO	geothermal
in	inlet
l	length
loss	losing
net	net power
out	outlet
pump	pumping
s	sun
sto	storage
tot	total
tur	turbine
U	useful
w	water
z	zenith
0	ambient

Abbreviations

EES	engineering equation solver
CT	cooling tower
HEX	heat exchanger
HHV	higher heating value
ORC	organic Rankine cycle
PEM	Proton Exchange Membrane
PTSC	parabolic trough solar collector

Introduction

As a result of the increase in electricity consumption, countries research to produce electricity from alternative sources today. Solar energy and geothermal resources stand out to generate electricity. Turkey can be considered as a lucky country in terms of geothermal and solar energy [1]. Geothermal resources can be divided into seven categories based on temperature. No direct electricity generation temperature, non-electrical grade (<100 °C), very low temperature (100 °C–150 °C), low temperature (150 °C–190 °C), moderate temperature (190 °C–230 °C), high temperature (230 °C–300 °C), ultra-high temperature (>300 °C) and steam field (approximately 240 °C with steam as the only mobile phase). Liquid water is the mobile phase in the first four classes of reservoirs; in "high" and "ultra-high" temperature reservoirs, the mobile liquid phase is either a liquid or a liquid-vapor mixture [2]. High-grade geothermal sources are widely used to generate electricity around the world. And also, electricity can be produced by ORC at very low-grade temperatures of geothermal source (<100 °C). So, the electricity generation from a very low-grade geothermal source is also a precious case. For this reason, electricity generation is also very important from low and middle-grade geothermal sources. The point to be considered here, if the temperature of the geothermal source is less than 50 °C, it is more suitable for space heating [3].

Literature review

ORC is an important system for generating electricity from low-grade geothermal sources when the working fluid is selected correctly [4]. Electricity generation is also possible from both medium and high-grade geothermal resources using ORC and different technologies [5]. In a parametric study, a geothermal source (130–200 °C) is used in a multi-generation system that consists of an ORC, a flash turbine, a cooling system, and a PEM system to generate electricity and hydrogen [6]. If these multi-generation systems are supported by solar radiation, electric energy generation can be improved [7]. The fluid temperature of a geothermal source can be upgraded through the solar collectors. Thus, the electricity can be generated more efficiently by using appropriate working fluids namely n-butane, n-hexane, and n-pentane in the ORC. It is found that n-butane performs better than the other two fluids. So, the working fluid in the ORC is extremely significant [8]. ORC and similar technologies need thermal energy to generate electricity. Therefore, such technologies like PTSCs are very important to convert solar energy into thermal energy [9]. The produced thermal energy by the PTSCs can be used for electricity generation by different technologies namely ORC, flash turbine, etc. [10]. For this purpose, PTSCs

are used in a multi-generation system for heating, cooling, drying, power and hydrogen production [11].

The electricity generation of the system can be improved even more by integrating the PTSCs with high-temperature geothermal sources and flash turbine. Thus, both power generation and exergy efficiency can be upgraded when comparing with the single systems [12]. For example, a geothermal resource (250 °C) is integrated with PTSCs for power and hydrogen production. As a result, it is found that much more power and hydrogen are produced [13]. Similarly, a geothermal resource (170 °C) is integrated with PTSCs for electricity generation and thermodynamic analyses. As a result, 12.76 MW of electricity is generated when n-pentane is operated in the ORC [14]. In another study, the temperature of the geothermal fluid is increased from 180 °C to 380 °C using PTSCs directly. In this work, a significant amount of hydrogen and electricity were produced. Hydrogen production rate can reach up to 2.648 kg/h for a day [15]. In another study, the temperature of the geothermal fluid is raised to a very high temperature using PTSCs, and electricity was generated in steam turbines. 26.38 kg of hydrogen is produced during the day by using this electricity [16]. In another study, two different systems are tested by integrating PTSCs and geothermal source. A considerable amount of hydrogen is produced in both systems [17]. Some parameters in these studies are summarized in Table 1.

The temperature of most of the geothermal resources in the world is below 150 °C [18]. Therefore, a high-grade fluid can be obtained by utilizing solar energy systems integrated with these sources and much more electricity can be produced compared to non-integrated geothermal sources. For example, a geothermal resource (150 °C) integrated and non-integrated with the PTSCs is compared to in terms of efficiency and the system integrated with the PTSCs is found to be 12% more efficient than the non-integrated system [19]. The efficiency of the systems is increased with the high-grade geothermal source. For example, the exergy efficiencies of a system that is used for power generation and cooling are calculated as 23.59%, 25.06%, and 26.25% for three different geothermal sources at 150, 160, and 170 °C, respectively [20]. The assessment of the efficiency of a system is very important for evaluating it thermodynamically [21]. The better understanding of the system performance, the exergy efficiency should be assessed instead of energy efficiency [22]. The power generation from a geothermal resource of 150 °C and below may not meet the cost of the system. Increasing the source depth to achieve high-grade geothermal fluid also increases the system cost [23]. Therefore, low-grade geothermal sources must be upgraded by auxiliary equipment like solar systems.

The excess electricity can be used to produce hydrogen for later use. Hydrogen is an efficient energy carrier. Thus, the aim of this study is to assess the power and hydrogen production of the integrated system that consists of PTSCs and ORC with a middle-grade geothermal source (150 °C) in Manisa. There are many studies on the thermodynamic analysis of the integrated systems comprise of PTSCs and a geothermal source. It is seen that the middle grade geothermal resources are quite abundant in the world. Since these sources have low energy, electricity and hydrogen production is costly. This study will contribute to the literature by increasing the energy and exergy of middle grade sources and producing more electricity and hydrogen. For this purpose, the best performance of the system is investigated by trying four different fluids in ORC. To determine the best option, the working fluids namely n-butane, n-pentane, n-hexane, and cyclohexane are calculated with four different mass flow rates. All analyzes in this article are done with Engineering Equation Solver (EES). How the system works and which equations are used for analysis are explained in the methodology section and the detailed results are given in the analysis section.

Case study region

The schematic of the integrated system is depicted in Fig. 1. The system consists of PTSCs, ORC, cooling towers, and a middle-grade geothermal source. The main aim of this integrated system is to produce much more thermal energy, power and hydrogen. For this purpose, the fluid of the middle-grade geothermal source is upgraded by PTSCs to operate the ORC. Thus, the electricity can be generated more efficiently. As shown in Fig. 1, the fluid of the geothermal source enters the PTSCs from point 2, and the upgraded fluid enters the evaporator from point 3 to operate the ORC. Electricity is then generated by the expansion of the vapor throughout the turbine. Thus, the generated electricity is delivered to PEM to produce hydrogen. The water required for electrolysis is obtained from the hot water tank. The condenser and cooling tower (CT) are used to remove the excess heat from the system. This system has been tested on a clear sunny day in July for Manisa province located at 37.96° north latitude. The instantaneous solar radiation and exergy on the surface of the collector are calculated using equations (7) and (12) and given in Table 2.

Methodology

The energetic and exergetic evaluation of the integrated system is assessed according to the thermodynamic principles. So, the balance equations for each component are derived to obtain the efficiency of the system.

The following acceptances are made for the analyses.

a) The ambient pressure is 101.3 atm.
b) The ambient temperature is 27.9 °C
c) Collectors have sun tracking system.
d) All processes take place according to the steady-state conditions.
e) Heat losses in connecting pipes are negligible.

Energy and exergy analyses of the PTSCs

The PTSCs are considered as a good solar technology that producing thermal energy. Some parts of the produced thermal energy in the PTSCs transfers to the geothermal fluid as useful energy while some parts are lost.

Table 1 – Energy and exergy efficiency of ORCs using different working fluids with different dimensions of PTSCs and geothermal source temperatures.

Geothermal temperature	The dimensions of the PTSCs	Working fluid ORC	Energy Eff. (%)	Exergy Eff. (%)	Reference
205–240 °C	12200–19600 m^2	Steam-liquid	–	33.95–41.78	[12]
250 °C	4 m × 50 m	Ammonia-water	78.37	58.40	[13]
170 °C	Unknown	n-pentane	10.74	23.90	[14]
180 °C	5.76 m × 12.27 m	R123	18.69	31.99	[15]
110 °C	5000–25000 m^2	Isobutane	–	21.63	[16]
423–489 K	5.22 m × 62 m	Steam	–	11.78	[17]

Energy balance equations for the PTSCs can be given as:

$$\dot{E}_{PTSCs} = \dot{E}_U + \dot{E}_{loss,PTSCs} \quad (1)$$

$$\dot{E}_{PTSCs} = \dot{I}_{bP} A_{PTSCs} \quad (2)$$

where $\dot{I}_{bP}$ is the direct solar radiation on the PTSCs, A_{PTSCs} (545 m^2) is the total surface area of the PTSCs. The useful energy ($\dot{E}_U$) for the PTSCs can be given as [24]:

$$\dot{E}_U = \dot{m}_w C_w (T_3 - T_2) \quad (3)$$

Table 2 – Solar radiation and exergy on the PTSCs.

Hours	Energy (W/m^2)	Exergy (W/m^2)
8–9	461.3	429.2
9–10	551.6	513.2
10–11	615.5	572.7
11–12	648.5	603.4
12–13	648.5	603.4
13–14	615.5	572.7
14–15	551.6	513.2
15–16	461.3	429.2
16–17	350.6	326.3

where $\dot{m}_w$ is the mass flow rate of the geothermal fluid, T_2 is the inlet temperature, T_3 is the outlet temperature and C_w is the specific heat of water.

The energy efficiency for the PTSCs can be given as:

$$\eta_{PTSCs} = \frac{\dot{E}_U}{\dot{E}_{PTSCs}} \quad (4)$$

$$\eta_{PTSCs} = \frac{\dot{m}_w C_w (T_3 - T_2)}{\dot{I}_{bP} A_{PTSCs}} \quad (5)$$

PTSCs have solar tracking system from east to west from. Also, the energy efficiency of the PTSCs can be calculated as [25]:

$$\eta_{PTSCs} = 0.69 - 0.39(T_{in} - T_0) \Big/ \dot{I}_{bP} \quad (6)$$

$$\dot{I}_{bP} = \dot{I}_b R_{bP} \quad (7)$$

$$R_{bP} = \frac{\cos\theta_{we}}{\cos\theta_z} \quad (8)$$

Angel of incident of the PTSC can be found [24]:

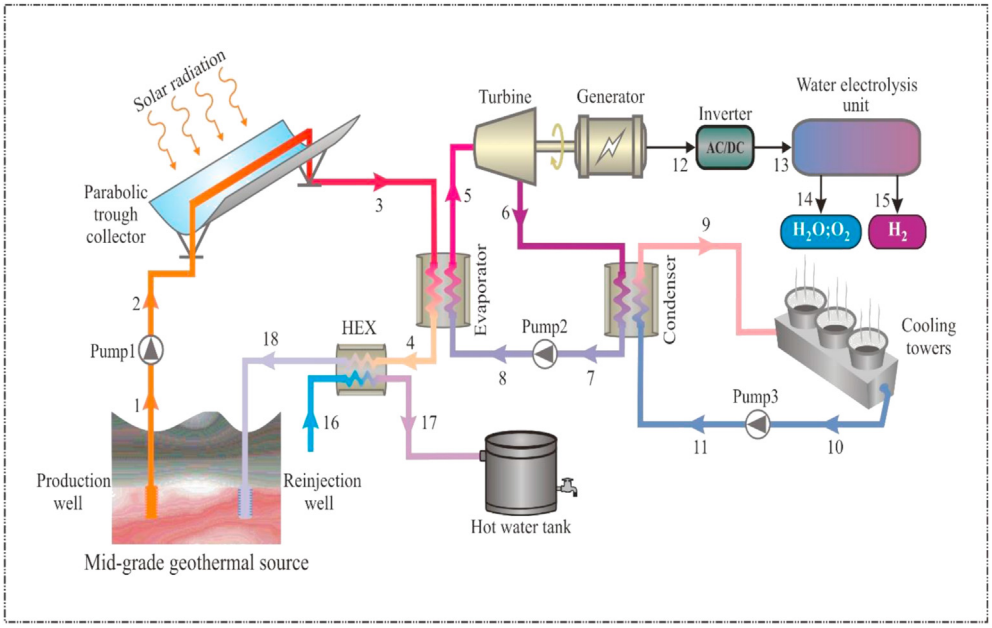

Fig. 1 – Schematic of the integrated system.

$$\cos\theta_{we} = \sqrt{1 - \cos^2\delta \sin^2 w} \tag{9}$$

$$\cos\theta_z = \sin\delta \sin\phi + \cos\delta \cos\phi \cos w \tag{10}$$

where T_{in} is the inlet temperature of the PTSCs, T_0 is the ambient temperature, $\dot{I}_b$ is the direct solar radiation, R_{bp} is the direct radiation coefficient, δ is the declination angle, $\varnothing$ is the latitude of the city and w is the hour angle.

The exergy of the direct solar radiation reaching the PTSCs is necessary to calculate the exergy efficiency of the PTSCs. Thus, solar exergy can be given as [26]:

$$\dot{E}x_{PTSCs} = \dot{I}x_{PTSCs} A_{PTSCs} \tag{11}$$

$$\dot{I}x_{PTSCs} = \dot{I}_{bP}\left[1 - \frac{4}{3}\left(\frac{T_0 + 273}{T_s}\right) + \frac{1}{3}\left(\frac{T_0 + 273}{T_s}\right)^4\right] \tag{12}$$

where T_S is the surface temperature of the sun ($T_S = 5770$ K).

$$\dot{E}x_{PTSCs} = \dot{E}x_U + \dot{E}x_{loss,PTSCs} + \dot{E}x_{dest,PTSCs} \tag{13}$$

where $\dot{E}x_U$ is the useful exergy, $\dot{E}x_{loss,PTSCs}$ is the exergy loss from the PTSCs and $\dot{E}x_{dest,PTSCs}$ is the exergy destruction of the PTSCs. Exergy useful for the PTSCs is written as follows:

$$\dot{E}x_U = \dot{m}_w C_w \left(T_3 - T_2 - T_0 \ln\frac{T_3}{T_2}\right) \tag{14}$$

The exergy efficiency for the PTSCs can be given as:

$$\psi_{PTSCs} = \frac{\dot{E}x_U}{\dot{E}x_{PTSCs}} = 1 - \frac{\dot{E}x_{dest,PTSCs} + \dot{E}x_{loss,PTSCs}}{\dot{E}x_{PTSCs}} \tag{15}$$

$$\psi_{PTSCs} = \frac{\dot{m}_w C_w \left(T_3 - T_2 - T_0 \ln\frac{T_3}{T_2}\right)}{\dot{I}_b\left[1 - \frac{4}{3}\left(\frac{T_0+273}{T_s}\right) + \frac{1}{3}\left(\frac{T_0+273}{T_s}\right)^4\right] A_{PTSCs}} \tag{16}$$

Analyses of the ORC

Energy analysis of the ORC

An ORC is a power generating device that including an evaporator, a condenser, a pump, a turbine, and a working fluid which evaporates at low temperature [27].

The net electricity generation for the ORC cycle can be given as:

$$\dot{W}_{net} = \dot{W}_G - \left(\dot{W}_{pump2}\right) \tag{17}$$

where $\dot{W}_G$ is the turbine power and it can be given as:

$$\dot{W}_G = \eta_{tur}\eta_G \dot{m}_5 (h_5 - h_6) \tag{18}$$

where η_{tur} and η_G are the efficiencies of the turbine and the generator, respectively. Thus, $\eta_{tur}\eta_G$ is taken as 0.25 in this system.

Where $\dot{W}_{pump2}$ is expressed as follows:

$$\dot{W}_{pump2} = \dot{m}_7 (h_8 - h_7) \tag{19}$$

Thus, energy efficiency for the ORC cycle can be given as:

$$\eta_{ORC} = \frac{\dot{W}_{net,ORC}}{\dot{Q}_{eva}} \tag{20}$$

where $\dot{Q}_{eva}$ is the input thermal energy from evaporator to the ORC that is calculated as follows:

$$\dot{Q}_{eva} = \dot{m}_5 (h_5 - h_8) \tag{21}$$

Exergy analysis of the ORC

To perform the exergy analysis, each component of the ORC is assessed. Therefore, exergy balance equations for the components of the ORC can be given as follows:

For evaporator:

$$\dot{E}x_3 + \dot{E}x_8 = \dot{E}x_5 + \dot{E}x_4 + \dot{E}x_{dest,eva} + \dot{E}x_{loss,eva} \tag{22}$$

where $\dot{E}x_3$ and $\dot{E}x_8$ are the inlet exergies, $\dot{E}x_4$ and $\dot{E}x_5$ are the outlet exergies of the evaporator and $\dot{E}x_{dest,eva}$ and $\dot{E}x_{loss,eva}$ represent the exergy destruction and exergy loss of the evaporator.

For turbine:

$$\dot{E}x_5 = \dot{E}x_6 + \dot{W}_G + \dot{E}x_{dest,tur} \tag{23}$$

where $\dot{E}x_5$ and $\dot{E}x_6$ are the inlet and outlet exergies of the turbine and $\dot{E}x_{dest,tur}$ is the exergy destruction, respectively.

For condenser:

$$\dot{E}x_6 + \dot{E}x_{11} = \dot{E}x_7 + \dot{E}x_9 + \dot{E}x_{dest,con} + \dot{E}x_{loss,con} \tag{24}$$

where $\dot{E}x_6$ and $\dot{E}x_{11}$ are the inlet exergies, $\dot{E}x_7$ and $\dot{E}x_9$ are the outlet exergies of the condenser, $\dot{E}x_{dest,con}$ and $\dot{E}x_{loss,con}$ represent the exergy destruction and exergy loss of the condenser.

For pump2:

$$\dot{E}x_7 + \dot{W}_{pump2} = \dot{E}x_8 + \dot{E}x_{dest,pump2} \tag{25}$$

Total exergy destruction for the ORC is written as:

$$\dot{E}x_{dest,ORC} = \dot{E}x_{dest,eva} + \dot{E}x_{dest,tur} + \dot{E}x_{dest,con} + \dot{E}x_{dest,pump2} \tag{26}$$

Thus, overall exergy efficiency for the ORC cycle is written as [28]:

$$\psi_{ORC} = \frac{\dot{W}_{net,ORC}}{\dot{E}x_{in,ORC}} = 1 - \frac{\dot{E}x_{loss,ORC} + \dot{E}x_{dest\ ORC}}{\dot{E}x_{in,ORC}} \tag{27}$$

Where $\dot{E}x_{in,ORC}$ is the inlet exergy for the ORC and it is written as:

$$\dot{E}x_{in,ORC} = \dot{m}_3[(h_3 - h_0) - T_0(s_3 - s_0)] \tag{28}$$

where h_3 and h_0 are the specific enthalpies at points 0 and 3. Similarly s_3 and s_0 are the specific entropies.

PEM electrolysis

PEM water electrolysis is a system that converts the electricity into hydrogen. In this system, water is electrochemically split into hydrogen and oxygen through PEM electrolysis. The chemical reaction for hydrogen production is given as [29]:

$$H_2O \rightarrow H_2 + 1/2O_2 \quad \Delta h = 285.84\ \text{kJ/mol} \tag{29}$$

The electricity requirement of the PEM can be given as following equation:

$$\Delta G = \Delta h - T\Delta S \tag{30}$$

where

$$\Delta S = S_{H_2} + \frac{1}{2}S_{O_2} - S_{H_2O} \tag{31}$$

$$\Delta H = H_{H_2} + \frac{1}{2}H_{O_2} - H_{H_2O} \tag{32}$$

The performance of the PEM can be found as follows [30]:

$$\eta_{PEM} = \frac{\Delta G}{\Delta H} \tag{33}$$

Also, the electrical efficiency of the PEM can be found as given [31]:

$$\eta_{PEM} = \frac{\dot{m}_{H_2} \times HHV}{\dot{W}_{PEM}} \tag{34}$$

The performance of the PEM varies between 60 and 80%. 285.84 kJ of electrical energy is used for electrolyzing of 1 mol water. As a result of the electrolysis 2 g of H_2 and 16 g O_2 can be produced according to Ref. [32]. In this study, efficiency of the PEM is taken as 80%.

Compressor

The energy and exergy analysis of the compressor can be found as follows:

Energy analysis

$$\dot{E}_{in,comp} + \dot{W}_{comp} = \dot{E}_{out,comp} \tag{35}$$

Exergy analysis

$$\dot{E}x_{in,comp} + \dot{W}_{comp} = \dot{E}x_{out,comp} + \dot{E}x_{dest,comp} \tag{36}$$

Overall exergy destruction of the integrated system

To assess the exergy efficiency of a system, the exergy destruction should be determined. Therefore, the overall exergy destruction is given as:

$$\dot{E}x_{dest,tot} = \dot{E}x_{dest,PTSCs} + \dot{E}x_{dest,eva} + \dot{E}x_{dest,tur} + \dot{E}x_{dest,con} + \dot{E}x_{dest,pumps} + \dot{E}x_{dest,cool} + \dot{E}x_{dest,PEM} + \dot{E}x_{dest,comp} + \dot{E}x_{dest,HEX} \tag{37}$$

where $\dot{E}x_{dest,pumps}$ and $\dot{E}x_{dest,cool}$ are the exergy destruction within the pumps and the cooling towers, respectively. They can be given as:

$$\dot{E}x_{dest,pumps} = \dot{E}x_{dest,pump1} + \dot{E}x_{dest,pump3} \tag{38}$$

$$\dot{E}x_{dest,cool} = \dot{E}x_9 - \dot{E}x_{10} \tag{39}$$

The inlet energy to the integrated system can be given as:

$$\dot{E}_{in} = \dot{E}_{GEO} + \dot{E}_{PTSCs} + \dot{E}_{cold,w} \tag{40}$$

The overall electrical energy efficiency for the system can be given as:

$$\eta_{overall} = \frac{\dot{E}_{use,sys}}{\dot{E}_{in}} \tag{41}$$

where, $\dot{E}_{use,sys}$ is the useful energy that is produced by the system and it can be found as follows:

$$\dot{E}_{use,sys} = \dot{m}_{H_2} \times HHV + \dot{E}_{CT} + \dot{E}_{H_2} + \dot{E}_{sto} \tag{42}$$

The inlet exergy to the integrated system is written as follows:

$$\dot{E}x_{in} = \dot{E}x_{GEO} + \dot{E}x_{PTSCs} + \dot{E}x_{cold,w} \tag{43}$$

And the overall electrical exergy efficiency is written as follows:

$$\psi_{overall} = \frac{\dot{E}_{use,sys}}{\dot{E}x_{in}} \tag{44}$$

where $\dot{E}x_{use,sys}$ is the useful exergy that is produced by the system and it can be found as follows:

$$\dot{E}x_{use} = \dot{m}_{H_2} \times HHV + \dot{E}x_{CT} + \dot{E}x_{H_2} + \dot{E}x_{sto} \tag{45}$$

Analysis

The fluid temperature from the middle-grade geothermal source is increased by using PTSCs that has a total area of 545 m^2. Therefore, the energy and exergy of the solar radiation reaching the surface of the PTSCs are calculated to evaluate the system thermodynamically. The temperature of the output fluid of the PTSCs depends on the amount of solar energy. Fig. 2 shows the hourly average energy and exergy distributions of solar radiation reaching the PTSCs and outlet temperature of the PTSCs from 8^{00} to 17^{00} h. The maximum and minimum direct solar radiations reaching the PTSCs are found as 353.4 kW and 191.1 kW between the hours of 11^{00}-13^{00} and 16^{00}-17^{00}, respectively. The maximum and minimum solar exergies reaching the PTSCs are found as 328.9 kW and 177.8 kW between the hours of 11^{00}-13^{00} and 16^{00}-17^{00}, respectively. The instant maximum and minimum outlet temperatures of the PTSCs are upgraded from 155 °C to 280.8 °C and from 155 °C to 213.8 °C between the hours of 11^{00}-13^{00} and 16^{00}-17^{00}, respectively. The fluctuation in solar energy also affects the temperature of the outlet fluid of the PTSCs during the day.

The solar energy and ambient temperature affect the efficiency of PTSCs. Fig. 3 shows the efficiency of the PTSCs depending on solar energy, inlet and ambient temperature. The maximum and minimum energy efficiencies of the PTSCs are calculated as 61.63% and 55.36% between the hours of 11^{00}-13^{00} and 16^{00}-17^{00}, respectively. The maximum and minimum

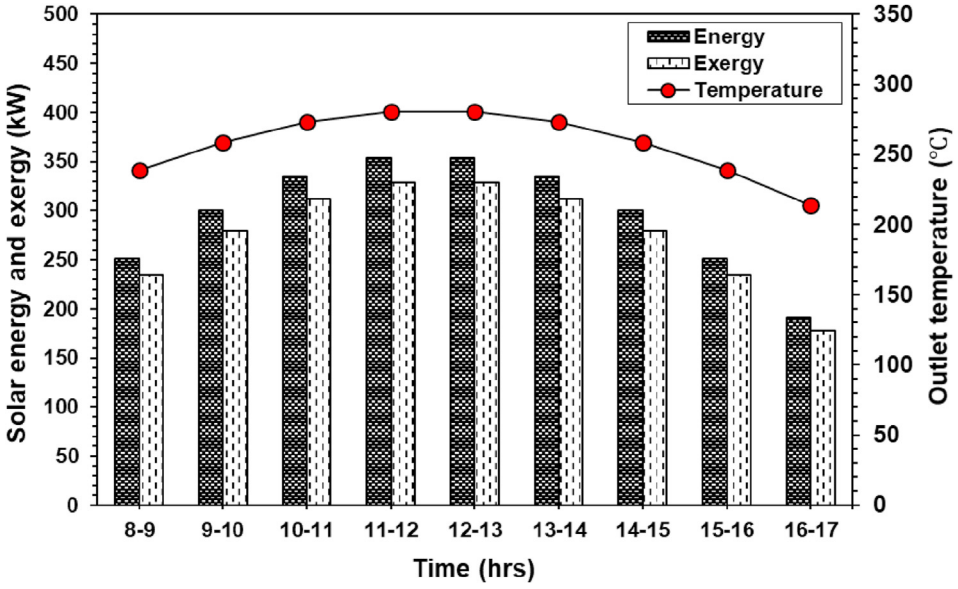

Fig. 2 – The daily solar energy and exergy, and outlet temperature distributions of the PTSCs.

exergy efficiencies of the PTSCs are calculated as 25.20% and 20.10% between the hours of 11^{00}-13^{00} and 16^{00}-17^{00}, respectively. The performance of the PTSCs increases from morning till noontime and decreases toward evening.

To make the thermodynamic analysis, the required parameters are given in Table 3. Knowing these parameters is very important to thermodynamic assessment. Some parameters of the system depending on the changes in temperature, pressure and solar energy have not given in this table.

To make the exergetic analysis, the exergy destruction of the components is listed in Tables 4–11. Thus, exergy destruction distribution for each working fluid is found for the system. Since solar energy and output temperature of the PTSCs are taken the same, the exergy destruction of the PTSCs is the same for each working fluid. When these tables are analyzed, the highest amount of exergy destruction is found in the ORC and then in the collectors. Exergy destruction in the other components is quite low compared to the ORC and collectors. The exergy destruction in the ORC and compressor increase when the mass flow rate of the working fluids increases from 0.1 kg/s to 0.4 kg/s for all configurations. Contrary, exergy destruction in the PEM decreases with increasing the mass flow rate of the working fluids. For the overall system, the total exergy destruction increases with increasing mass flow rate of the working fluids. The highest amount of exergy destruction is found for the configuration of n-butane with a mass flow rate of 0.4 kg/s. The lowest amount of exergy

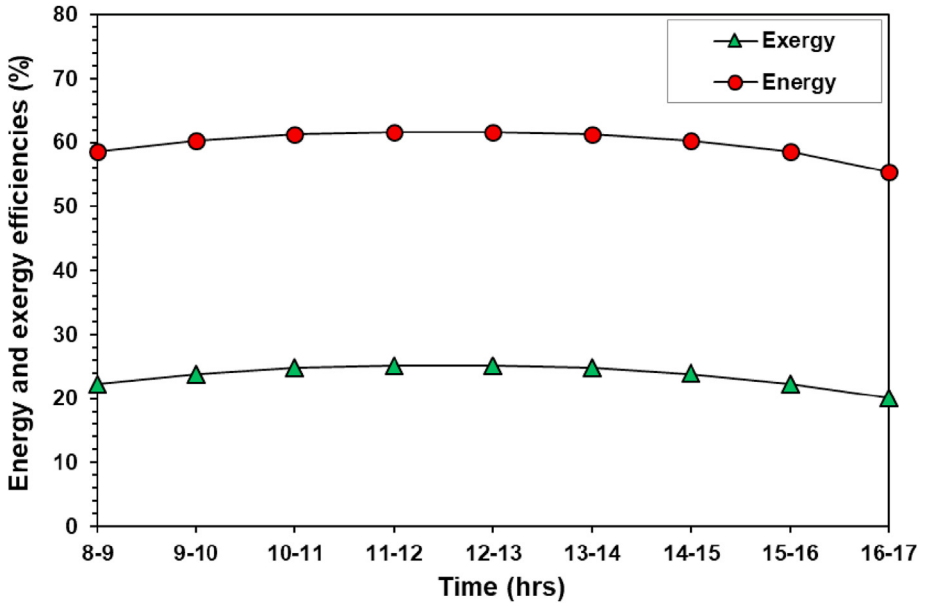

Fig. 3 – The daily energy and exergy efficiency distributions of the PTSCs.

Table 3 – Some parameters related to the integrated system.

Num.	Fluid	Temp. (^{0}C)	Pressure (kPa)	Mass flow rate (kg/s)	Enthalpy (kJ/kg)	Entropy (kJ/kg K)	Exergy (kJ/kg)
0	H_2O	27.9	101.3	0.4	117	0.407	–
1	H_2O	150	475	0.4	2746	6.839	694.2
2	H_2O	150.5	475	0.4	2748	6.842	694.6
3	H_2O	–	1500	0.4	–	–	–
4	H_2O	100	150	0.4	419.1	1.307	31.49
5	Fluid	T_3-20	2000	0.1–0.4	–	–	–
6	n-butane	100	1750	0.1–0.4	462.3	1.803	62.92
7	n-butane	80	1750	0.1–0.4	403.4	1.641	52.82
8	n-butane	80.5	2000	0.1–0.4	404.8	1.643	53.44
6′	n-pentane	100	1750	0.1–0.4	187.0	0.550	21.96
7′	n-pentane	80	1750	0.1–0.4	133.8	0.404	12.85
8′	n-pentane	80.5	2000	0.1–0.4	135.2	0.406	13.44
6″	n-hexane	100	1750	0.1–0.4	180.6	0.531	20.62
7″	n-hexane	80	1750	0.1–0.4	131.4	0.396	12.19
8″	n-hexane	80.5	2000	0.1–0.4	132.8	0.399	12.75
6‴	cyclohexane	100	1750	0.1–0.4	186.8	0.565	17.97
7‴	cyclohexane	80	1750	0.1–0.4	142.9	0.444	10.45
8‴	cyclohexane	80.5	2000	0.1–0.4	144.1	0.447	10.93
9	H_2O	95	100	0.04	398	1.250	27.47
10	H_2O	75	100	0.04	314	1.015	14.07
11	H_2O	75.5	100	0.04	316.1	1.021	14.35

Table 4 – Exergy destruction in the integrated system for different mass flow rates of n-butane.

Hours	$\dot{m} = 0.1$ kg/s								$\dot{m} = 0.2$ kg/s							
	Power of the components (kW)															
	PTSCs	ORC	PEM	HEX	Cool.	Comp.	Pumps	Total	ORC	PEM	HEX	Cool.	Comp.	Pumps	Total
8-9	144.6	64.48	28.39	2.103	0.536	0.502	0.398	241	67.42	28.13	2.103	0.536	1.026	0.398	244.2
9-10	168.9	51.54	28.37	2.103	0.536	0.555	0.398	252.4	55.79	28.08	2.103	0.536	1.132	0.398	257
10-11	185.5	42.76	28.35	2.103	0.536	0.593	0.398	260.2	48.03	28.04	2.103	0.536	1.208	0.398	265.8
11-12	193.9	38.34	28.34	2.103	0.536	0.613	0.398	264.2	44.16	28.02	2.103	0.536	1.248	0.398	270.3
12-13	193.9	38.34	28.34	2.103	0.536	0.613	0.398	264.2	44.16	28.02	2.103	0.536	1.248	0.398	270.3
13-14	185.5	42.76	28.35	2.103	0.536	0.593	0.398	260.2	48.03	28.04	2.103	0.536	1.208	0.398	265.8
14-15	168.9	51.54	28.37	2.103	0.536	0.555	0.398	252.4	55.79	28.08	2.103	0.536	1.132	0.398	257
15-16	144.6	64.48	28.39	2.103	0.536	0.502	0.398	241	67.42	28.13	2.103	0.536	1.026	0.398	244.2
16-17	113.2	81.2	28.43	2.103	0.536	0.439	0.398	226.3	82.71	28.2	2.103	0.536	0.8997	0.398	228

destruction is found for the configuration of cyclohexane with a mass flow rate of 0.4 kg/s.

The net electricity generation of the ORC for the day July 1st depending on the solar radiation reaching the PTSCs is listed in Tables 12 and 13. The net electricity generations of the 16 configurations that consist of four different fluids with four different mass flow rates are compared. As the mass flow rate in ORC increased, the amount of electricity produced by the

Table 5 – Exergy destruction in the integrated system for different mass flow rates of n-butane.

Hours	$\dot{m} = 0.3$ kg/s								$\dot{m} = 0.4$ kg/s							
	Power of the components (kW)															
	PTSCs	ORC	PEM	HEX	Cool.	Comp.	Pumps	Total	ORC	PEM	HEX	Cool.	Comp.	Pumps	Total
8–9	144.6	70.36	27.87	2.103	0.536	1.55	0.398	247.4	73.3	27.61	2.103	0.536	2.074	0.398	250.6
9–10	168.9	60.05	27.79	2.103	0.536	1.709	0.398	261.5	64.3	27.5	2.103	0.536	2.285	0.398	266.1
10–11	185.5	53.3	27.74	2.103	0.536	1.822	0.398	271.4	58.57	27.43	2.103	0.536	2.437	0.398	277
11–12	193.9	49.98	27.71	2.103	0.536	1.882	0.398	276.5	55.8	27.39	2.103	0.536	2.516	0.398	282.6
12–13	193.9	49.98	27.71	2.103	0.536	1.882	0.398	276.5	55.8	27.39	2.103	0.536	2.516	0.398	282.6
13–14	185.5	53.3	27.74	2.103	0.536	1.822	0.398	271.4	58.57	27.43	2.103	0.536	2.437	0.398	277
14–15	168.9	60.05	27.79	2.103	0.536	1.709	0.398	261.5	64.3	27.5	2.103	0.536	2.285	0.398	266.1
15–16	144.6	70.36	27.87	2.103	0.536	1.55	0.398	247.4	73.3	27.61	2.103	0.536	2.074	0.398	250.6
16–17	113.2	84.23	27.97	2.103	0.536	1.36	0.398	229.8	85.75	27.74	2.103	0.536	1.82	0.398	231.5

Table 6 – Exergy destruction in the integrated system for different mass flow rates of n-pentane.

Hours	$\dot{m}$ = 0.1 kg/s								$\dot{m}$ = 0.2 kg/s						
	Power of the components (kW)														
	PTSCs	ORC	PEM	HEX	Cool.	Comp.	Pumps	Total	ORC	PEM	HEX	Cool.	Comp.	Pumps	Total
8–9	144.6	64.39	28.4	2.103	0.536	0.497	0.398	240.9	67.24	28.14	2.103	0.536	1.015	0.398	244
9–10	168.9	51.44	28.37	2.103	0.536	0.5512	0.398	252.3	55.59	28.08	2.103	0.536	1.123	0.398	256.8
10–11	185.5	42.65	28.35	2.103	0.536	0.5899	0.398	260.1	47.81	28.05	2.103	0.536	1.201	0.398	265.6
11–12	193.9	38.23	28.34	2.103	0.536	0.610	0.398	264.1	43.93	28.03	2.103	0.536	1.241	0.398	270.1
12–13	193.9	38.23	28.34	2.103	0.536	0.610	0.398	264.1	43.93	28.03	2.103	0.536	1.241	0.398	270.1
13–14	185.5	42.65	28.35	2.103	0.536	0.5899	0.398	260.1	47.81	28.05	2.103	0.536	1.201	0.398	265.6
14–15	168.9	51.44	28.37	2.103	0.536	0.5512	0.398	252.3	55.59	28.08	2.103	0.536	1.123	0.398	256.8
15–16	144.6	64.39	28.4	2.103	0.536	0.497	0.398	240.9	67.24	28.14	2.103	0.536	1.015	0.398	244
16–17	113.2	81.12	28.43	2.103	0.536	0.4305	0.398	226.2	82.57	28.21	2.103	0.536	0.882	0.398	227.9

Table 7 – Exergy destruction in the integrated system for different mass flow rates of n-pentane.

Hours	$\dot{m}$ = 0.3 kg/s								$\dot{m}$ = 0.4 kg/s						
	Power of the components (kW)														
	PTSCs	ORC	PEM	HEX	Cool.	Comp.	Pumps	Total	ORC	PEM	HEX	Cool.	Comp.	Pumps	Total
8–9	144.6	70.09	27.88	2.103	0.536	1.533	0.398	247.1	72.94	27.62	2.103	0.536	2.051	0.398	250.2
9–10	168.9	59.74	27.8	2.103	0.536	1.695	0.398	261.2	63.9	27.51	2.103	0.536	2.268	0.398	265.6
10–11	185.5	52.97	27.74	2.103	0.536	1.811	0.398	271.1	58.13	27.44	2.103	0.536	2.422	0.398	276.5
11–12	193.9	49.64	27.71	2.103	0.536	1.872	0.398	276.1	55.35	27.4	2.103	0.536	2.503	0.398	282.2
12–13	193.9	49.64	27.71	2.103	0.536	1.872	0.398	276.1	55.35	27.4	2.103	0.536	2.503	0.398	282.2
13–14	185.5	52.97	27.74	2.103	0.536	1.811	0.398	271.1	58.13	27.44	2.103	0.536	2.422	0.398	276.5
14–15	168.9	59.74	27.8	2.103	0.536	1.695	0.398	261.2	63.9	27.51	2.103	0.536	2.268	0.398	265.6
15–16	144.6	70.09	27.88	2.103	0.536	1.533	0.398	247.1	72.94	27.62	2.103	0.536	2.051	0.398	250.2
16–17	113.2	84.02	27.98	2.103	0.536	1.333	0.398	229.5	85.47	27.75	2.103	0.536	1.785	0.398	231.2

ORC increased considerably. The properties of the working fluid in the ORC are crucial for power generation. When these tables are examined, the highest amount of net electricity generation is found for the configuration of n-butane with a mass flow rate of 0.4 kg/s between the hours of 11^{00}-13^{00}. The lowest amount of net electricity generation is found for the configuration of cyclohexane with a mass flow rate of 0.1 kg/s around 17^{00} o'clock due to the decreasing solar radiation.

The ambient temperature, geothermal source temperature, solar radiation reaching the PTSCs, pressure and kind of working fluid mainly affects the performance of the ORC. For this reason, the energy efficiency of the ORC is examined for each working fluid and the other parameters kept constant. Fig. 4 show the thermal energy efficiency of the ORC.

- The highest thermal energy efficiency is found as 22.82% for the configuration of n-butane between the hours of 11^{00}-13^{00}.
- The lowest thermal energy efficiency is found as 21.10% for the same fluid configuration between the hours of 16^{00}-17^{00}.
- The highest thermal energy efficiency is found as 22.99% for the configuration of n-pentane between the hours of 11^{00}-13^{00}. The lowest thermal energy efficiency is found as 22.28% for the same configuration between the hours of 16^{00}-17^{00}.
- The highest thermal energy efficiency is found as 23.09% for the configuration of n-hexane between the hours of 11^{00}-13^{00}. The lowest thermal energy efficiency is found as

Table 8 – Exergy destruction in the integrated system for different mass flow rates of n-hexane.

Hours	$\dot{m}$ = 0.1 kg/s								$\dot{m}$ = 0.2 kg/s						
	Power of the components (kW)														
	PTSCs	ORC	PEM	HEX	Cool.	Comp.	Pumps	Total	ORC	PEM	HEX	Cool.	Comp.	Pumps	Total
8-9	144.6	64.25	28.41	2.103	0.536	0.475	0.398	240.8	66.96	28.16	2.103	0.536	0.971	0.398	243.7
9-10	168.9	51.28	28.38	2.103	0.536	0.535	0.398	252.2	55.28	28.1	2.103	0.536	1.091	0.398	256.4
10-11	185.5	42.49	28.36	2.103	0.536	0.576	0.398	260	47.49	28.06	2.103	0.536	1.173	0.398	265.3
11-12	193.9	38.06	28.35	2.103	0.536	0.597	0.398	263.9	43.61	28.04	2.103	0.536	1.215	0.398	269.8
12-13	193.9	38.06	28.35	2.103	0.536	0.597	0.398	263.9	43.61	28.04	2.103	0.536	1.215	0.398	269.8
13-14	185.5	42.49	28.36	2.103	0.536	0.576	0.398	260	47.49	28.06	2.103	0.536	1.173	0.398	265.3
14-15	168.9	51.28	28.38	2.103	0.536	0.535	0.398	252.2	55.28	28.1	2.103	0.536	1.091	0.398	256.4
15-16	144.6	64.25	28.41	2.103	0.536	0.475	0.398	240.8	66.96	28.16	2.103	0.536	0.971	0.398	243.7
16-17	113.2	80.73	28.53	2.103	0.536	0.227	0.398	225.7	81.79	28.41	2.103	0.536	0.475	0.398	226.9

Table 9 – Exergy destruction in the integrated system for different mass flow rates of n-hexane.

Hours	$\dot{m}$ = 0.3 kg/s								$\dot{m}$ = 0.4 kg/s						
	Power of the components (kW)														
	PTSCs	ORC	PEM	HEX	Cool.	Comp.	Pumps	Total	ORC	PEM	HEX	Cool.	Comp.	Pumps	Total
8–9	144.6	69.67	27.91	2.103	0.536	1.467	0.398	246.7	72.37	27.66	2.103	0.536	1.963	0.398	249.6
9–10	168.9	59.28	27.82	2.103	0.536	1.647	0.398	260.7	63.28	27.54	2.103	0.536	2.203	0.398	265
10–11	185.5	52.49	27.76	2.103	0.536	1.77	0.398	270.6	57.49	27.46	2.103	0.536	2.367	0.398	275.9
11–12	193.9	49.15	27.73	2.103	0.536	1.834	0.398	275.6	54.7	27.42	2.103	0.536	2.452	0.398	281.5
12–13	193.9	49.15	27.73	2.103	0.536	1.834	0.398	275.6	54.7	27.42	2.103	0.536	2.452	0.398	281.5
13–14	185.5	52.49	27.76	2.103	0.536	1.77	0.398	270.6	57.49	27.46	2.103	0.536	2.367	0.398	275.9
14–15	168.9	59.28	27.82	2.103	0.536	1.647	0.398	260.7	63.28	27.54	2.103	0.536	2.203	0.398	265
15–16	144.6	69.67	27.91	2.103	0.536	1.467	0.398	246.7	72.37	27.66	2.103	0.536	1.963	0.398	249.6
16–17	113.2	82.84	28.28	2.103	0.536	0.723	0.398	228.1	83.9	28.16	2.103	0.536	0.972	0.398	229.2

Table 10 – Exergy destruction in the integrated system for different mass flow rates of cyclohexane.

Hours	$\dot{m}$ = 0.1 kg/s								$\dot{m}$ = 0.2 kg/s						
	Power of the components (kW)														
	PTSCs	ORC	PEM	HEX	Cool.	Comp.	Pumps	Total	ORC	PEM	HEX	Cool.	Comp.	Pumps	Total
8–9	144.6	63.36	28.51	2.103	0.536	0.268	0.398	239.8	65.17	28.37	2.103	0.536	0.5569	0.398	241.7
9–10	168.9	51.12	28.38	2.103	0.536	0.5225	0.398	252	54.96	28.11	2.103	0.536	1.066	0.398	256.1
10–11	185.5	42.3	28.37	2.103	0.536	0.5618	0.398	259.8	47.1	28.07	2.103	0.536	1.144	0.398	264.9
11–12	193.9	37.85	28.36	2.103	0.536	0.5817	0.398	263.7	43.18	28.05	2.103	0.536	1.184	0.398	269.3
12–13	193.9	37.85	28.36	2.103	0.536	0.5817	0.398	263.7	43.18	28.05	2.103	0.536	1.184	0.398	269.3
13–14	185.5	42.3	28.37	2.103	0.536	0.5618	0.398	259.8	47.1	28.07	2.103	0.536	1.144	0.398	264.9
14–15	168.9	51.12	28.38	2.103	0.536	0.5225	0.398	252	54.96	28.11	2.103	0.536	1.066	0.398	256.1
15–16	144.6	63.36	28.51	2.103	0.536	0.268	0.398	246.7	72.37	27.66	2.103	0.536	1.963	0.398	241.7
16–17	113.2	80.62	28.55	2.103	0.536	0.1991	0.398	228.1	83.9	28.16	2.103	0.536	0.9719	0.398	226.6

20.72% for the same fluid configuration of n-hexane between the hours of 16^{00}-17^{00}.

- The highest thermal energy efficiency is found as 23.24% for the configuration of cyclohexane between the hours of 11^{00}-13^{00}. The lowest thermal energy efficiency is found as 20.70% for the same configuration between the hours of 16^{00}-17^{00}.

When the thermal energy performance of the ORC is examined, it is found that the working fluids show slightly different performance compared to each other. While the energy performance of the ORC increases towards noon for all fluids, its performance decreases in the afternoon.

The exergetic performance of the ORC depends on the kind of working fluid, exergies of the solar radiation and geothermal fluid, ambient temperature, and pressure. For this reason, the exergy efficiency of the ORC is examined for each working fluid and the other parameters kept constant. Figs. 5 and 6 show the overall exergy efficiency of the ORC for the working fluids.

- The highest exergy efficiency is found as 17.54% for the configuration of n-butane with $\dot{m}$ = 0.4 kg/s between the hours of 11^{00}-13^{00}. The lowest exergy efficiency is found as 3.42% for the same fluid configuration with $\dot{m}$ = 0.1 kg/s between the hours of 16^{00}-17^{00}.
- The highest exergy efficiency is found as 17.44% for the configuration of n-pentane with $\dot{m}$ = 0.4 kg/s between the hours of 11^{00}-13^{00}. The lowest exergy efficiency is found as 3.36% for the same fluid configuration with $\dot{m}$ = 0.1 kg/s between the hours of 16^{00}-17^{00}.

Table 11 – Exergy destruction in the integrated system for different mass flow rates of cyclohexane.

Hours	$\dot{m}$ = 0.3 kg/s								$\dot{m}$ = 0.4 kg/s						
	Power of the components (kW)														
	PTSCs	ORC	PEM	HEX	Cool.	Comp.	Pumps	Total	ORC	PEM	HEX	Cool.	Comp.	Pumps	Total
8–9	144.6	66.97	28.22	2.103	0.536	0.8458	0.398	243.7	68.78	28.08	2.103	0.536	1.135	0.398	245.6
9–10	168.9	58.8	27.84	2.103	0.536	1.609	0.398	260.2	62.64	27.57	2.103	0.536	2.152	0.398	264.3
10–11	185.5	51.91	27.78	2.103	0.536	1.727	0.398	270	56.71	27.49	2.103	0.536	2.31	0.398	275.1
11–12	193.9	48.51	27.75	2.103	0.536	1.787	0.398	275	53.83	27.45	2.103	0.536	2.389	0.398	280.6
12–13	193.9	48.51	27.75	2.103	0.536	1.787	0.398	275	53.83	27.45	2.103	0.536	2.389	0.398	280.6
13–14	185.5	51.91	27.78	2.103	0.536	1.727	0.398	270	56.71	27.49	2.103	0.536	2.31	0.398	275.1
14–15	168.9	58.8	27.84	2.103	0.536	1.609	0.398	260.2	62.64	27.57	2.103	0.536	2.152	0.398	264.3
15–16	144.6	66.97	28.22	2.103	0.536	0.8458	0.398	243.7	68.78	28.08	2.103	0.536	1.135	0.398	245.6
16–17	113.2	82.5	28.33	2.103	0.536	0.639	0.398	227.7	83.44	28.22	2.103	0.536	0.859	0.398	228.7

Table 12 – Net electricity generation (kW) of the ORC for n-butane and n-pentane.

Hours	n-butane				n-pentane			
	Mass flow rates (kg/s)							
	$\dot{m} = 0.1$	$\dot{m} = 0.2$	$\dot{m} = 0.3$	$\dot{m} = 0.4$	$\dot{m} = 0.1$	$\dot{m} = 0.2$	$\dot{m} = 0.3$	$\dot{m} = 0.4$
8–9	13.63	27.25	40.88	54.5	13.48	26.95	40.43	53.91
9–10	15	30	45	60	14.89	29.77	44.66	59.55
10–11	15.99	31.98	47.96	63.95	15.89	31.78	47.68	63.57
11–12	16.51	33.01	49.52	66.02	16.42	32.83	49.25	65.66
12–13	16.51	33.01	49.52	66.02	16.42	32.83	49.25	65.66
13–14	15.99	31.98	47.96	63.95	15.89	31.78	47.68	63.57
14–15	15	30	45	60	14.89	29.77	44.66	59.55
15–16	13.63	27.25	40.88	54.5	13.48	26.95	40.43	53.91
16–17	11.98	23.95	35.93	47.91	11.75	23.49	35.24	46.98

Table 13 – Net electricity generation (kW) of the ORC for n-hexane and cyclohexane.

Hours	n-hexane				Cyclohexane			
	Mass flow rates (kg/s)							
	$\dot{m} = 0.1$	$\dot{m} = 0.2$	$\dot{m} = 0.3$	$\dot{m} = 0.4$	$\dot{m} = 0.1$	$\dot{m} = 0.2$	$\dot{m} = 0.3$	$\dot{m} = 0.4$
8-9	12.9	25.81	38.71	51.62	7.517	15.03	22.55	28.44
9-10	14.46	28.93	43.39	57.86	14.14	28.28	42.41	53.94
10-11	15.53	31.07	46.6	62.14	15.16	30.32	45.48	57.89
11-12	16.09	32.17	48.26	64.34	15.68	31.36	47.04	59.88
12-13	16.09	32.17	48.26	64.34	15.68	31.36	47.04	59.88
13-14	15.53	31.07	46.6	62.14	15.16	30.32	45.48	57.89
14-15	14.46	28.93	43.39	57.86	14.14	28.28	42.41	53.94
15-16	12.9	25.81	38.71	51.62	7.517	15.03	22.55	28.44
16-17	6.458	12.92	19.37	25.83	5.723	11.45	17.17	21.53

- The highest exergy efficiency is found as 17.09% for the configuration of n-hexane with $\dot{m} = 0.4$ kg/s between the hours of 11^{00}-13^{00}. The lowest exergy efficiency is found as 1.84% for the same fluid configuration with $\dot{m} = 0.1$ kg/s between the hours of 16^{00}-17^{00}.
- The highest exergy efficiency is found as 16.66% for the configuration of cyclohexane with $\dot{m} = 0.4$ kg/s between the hours of 11^{00}-13^{00}. The lowest exergy efficiency is found as 1.63% for the same fluid configuration $\dot{m} = 0.1$ kg/s between the hours of 16^{00}-17^{00}.

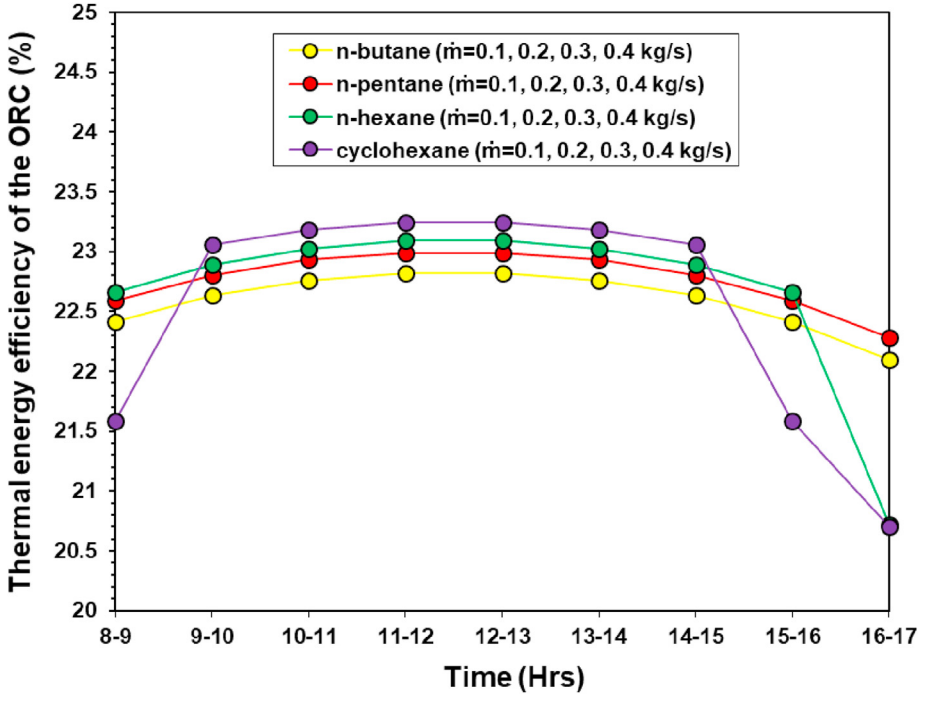

Fig. 4 – The thermal energy efficiency of the ORC for four fluids for a day.

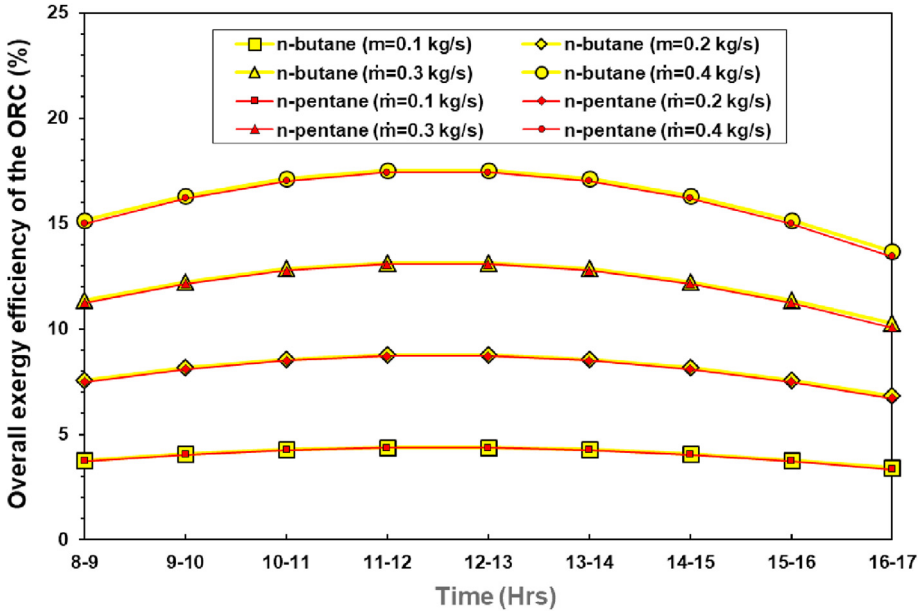

Fig. 5 – The overall exergy efficiency of the ORC for n-butane and n-pentane for a day.

Thus, it is found that the working fluids show different exergetic performance compared to each other. The exergy efficiency of the ORC highly increases with increasing of the mass flow rate from 0.1 kg/s to 0.4 kg/s. Among the four fluids, n-butane performs the best.

Figs. 7 and 8 show the overall energy efficiency of the integrated system regarding the working fluids in the ORC.

- The highest overall energy efficiency is found as 5.85% for the configuration of n-butane with $\dot{m} = 0.4$ kg/s between the hours of 11^{00}-13^{00}. The lowest energy efficiency is found as 3.22% for the same fluid configuration with $\dot{m} = 0.1$ kg/s between the hours of 8^{00}-9^{00}.
- The highest overall energy efficiency is found as 5.83% for the configuration of n-pentane with $\dot{m} = 0.4$ kg/s between the hours of 11^{00}-13^{00}. The lowest energy efficiency is found as 3.21% for the same fluid configuration with $\dot{m} = 0.1$ kg/s between the hours of 8^{00}-9^{00}.
- The highest overall energy efficiency is found as 5.76% for the configuration of n-hexane with $\dot{m} = 0.4$ kg/s between the hours of 11^{00}-13^{00}. The lowest energy efficiency is

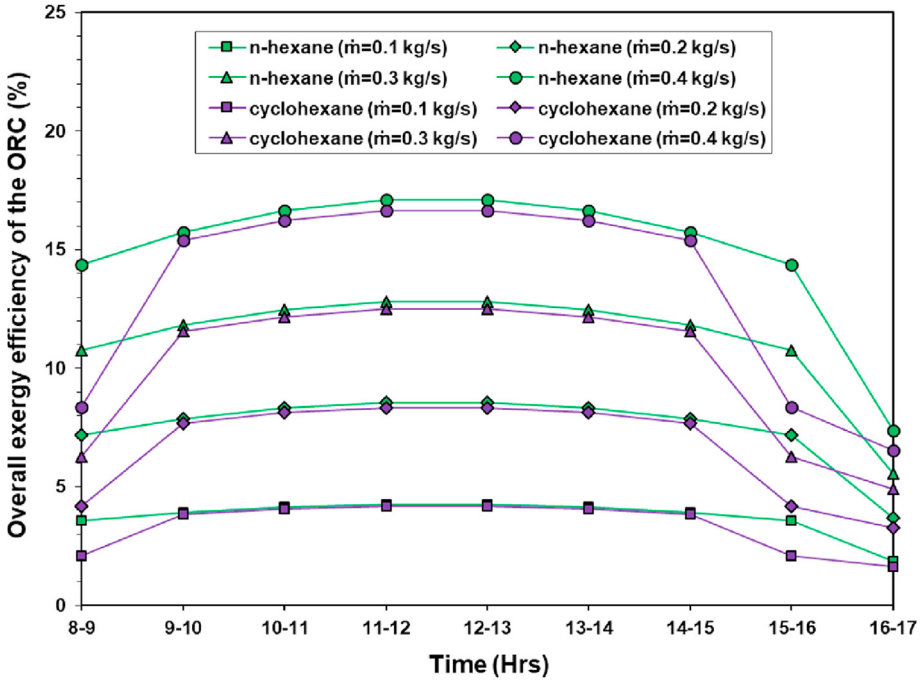

Fig. 6 – The overall exergy efficiency of the ORC for n-hexane and cyclohexane for a day.

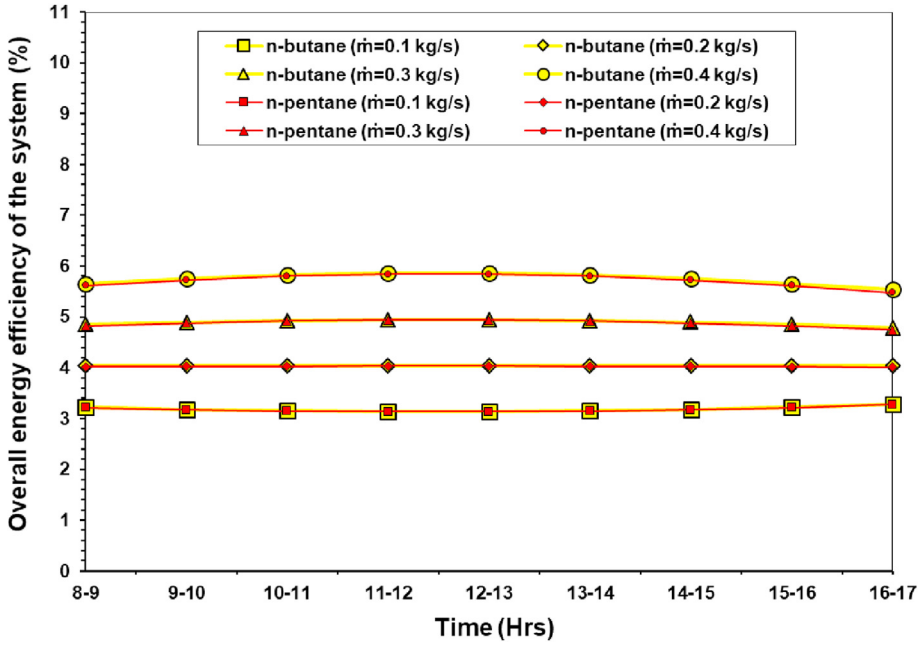

Fig. 7 – The overall energy efficiency of the integrated system for the working fluids in the ORC.

found as 2.94% for the same fluid configuration with $\dot{m} = 0.1$ kg/s between the hours of 16^{00}-17^{00}.

- The highest overall energy efficiency is found as 5.67% for the configuration of cyclohexane with $\dot{m} = 0.4$ kg/s between the hours of 11^{00}-13^{00}. The lowest energy efficiency is found as 2.86% for the same fluid configuration with $\dot{m} = 0.1$ kg/s between the hours of 8^{00}-9^{00}.

Thus, it was found that the working fluids show a slightly different performance compared to each other. The overall energy efficiency of the system increases with the increasing of the mass flow rate from 0.1 kg/s to 0.4 kg/s. Among the four fluids, n-butane performs the best.

Figs. 10 and 11 show the overall exergy efficiencies of the integrated system regarding the working fluids in the ORC.

- The highest overall exergy efficiency is found as 8.27% for the configuration of n-butane with $\dot{m} = 0.4$ kg/s between the hours of 11^{00}-13^{00}. The lowest exergy efficiency is found

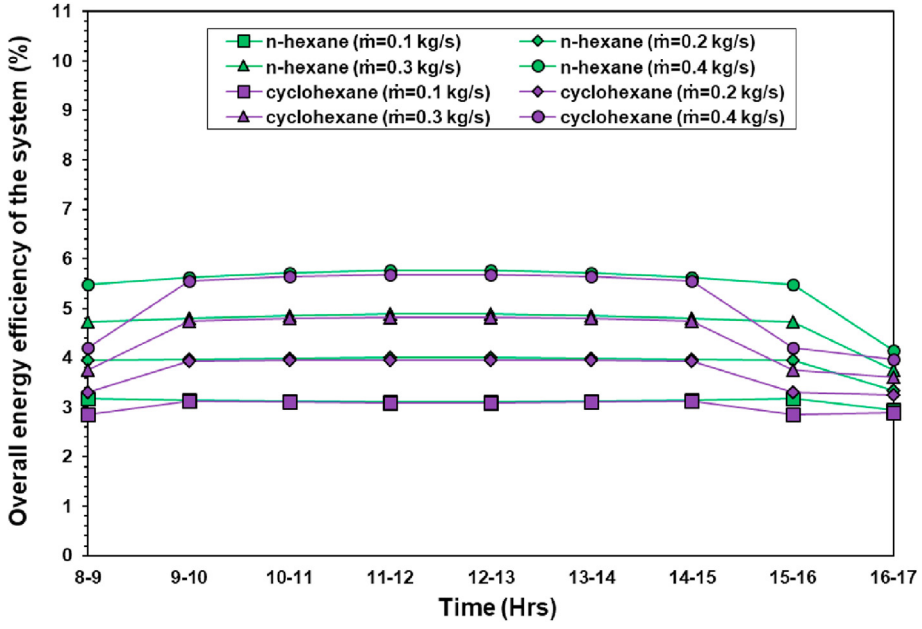

Fig. 8 – The overall energy efficiency of the integrated system for the working fluids in the ORC.

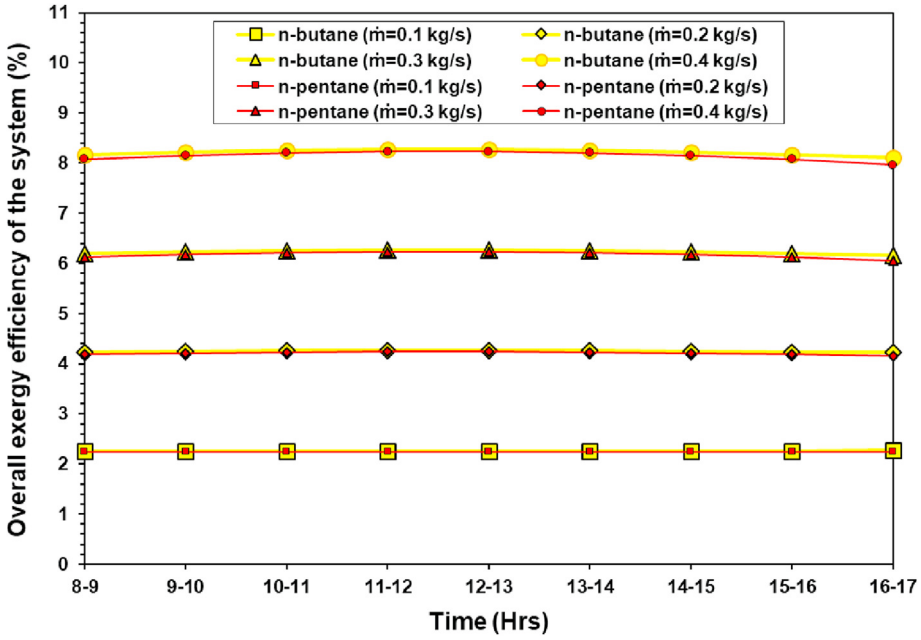

Fig. 9 – The overall exergy efficiency of the integrated system for the n-butane and n-pentane.

as 2.26% for the same fluid configuration with $\dot{m} = 0.1$ kg/s between the hours of 8^{00}-9^{00}.

- The highest overall exergy efficiency is found as 8.22% for the configuration of n-pentane with $\dot{m} = 0.4$ kg/s between the hours of 11^{00}-13^{00}. The lowest exergy efficiency is found as 2.24% for the same fluid configuration with $\dot{m} = 0.1$ kg/s between the hours of 16^{00}-17^{00}.
- The highest overall exergy efficiency is found as 8.06% for the configuration of n-hexane with $\dot{m} = 0.4$ kg/s between the hours of 11^{00}-13^{00}. The lowest exergy efficiency is found as 1.38% for the configuration of n-hexane with $\dot{m} = 0.1$ kg/s between the hours of 16^{00}-17^{00}.
- The highest overall exergy efficiency is found as 7.86% for the configuration of cyclohexane with $\dot{m} = 0.4$ kg/s between the hours of 11^{00}-13^{00}. The lowest exergy efficiency is found as 1.26% for the same fluid configuration with $\dot{m} = 0.1$ kg/s between the hours of 16^{00}-17^{00}.

Thus, it is found that the working fluids show a slightly different performance compared to each other. The overall exergy efficiency of the system increases with the increasing

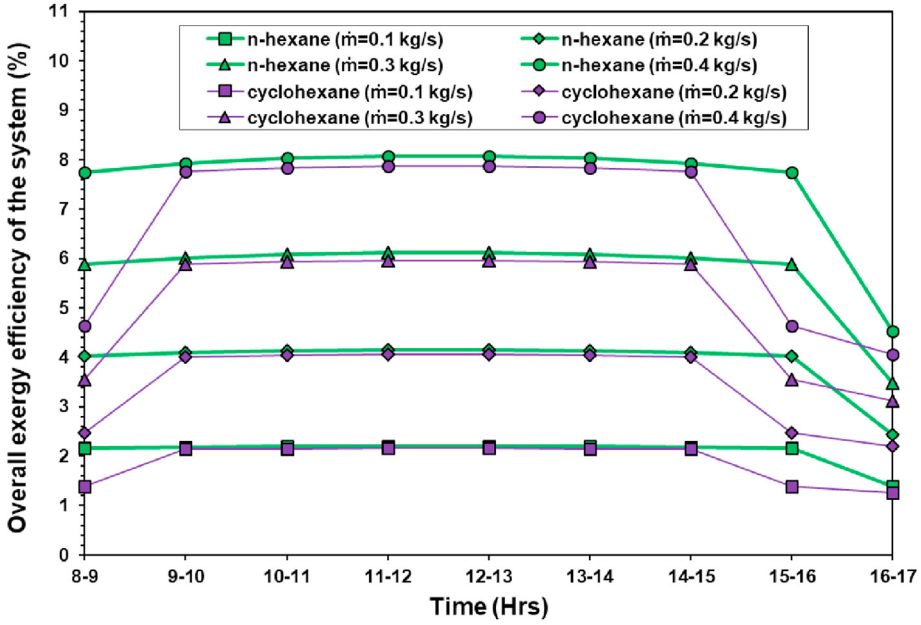

Fig. 10 – The overall exergy efficiency of the integrated system for the n-hexane and cyclohexane.

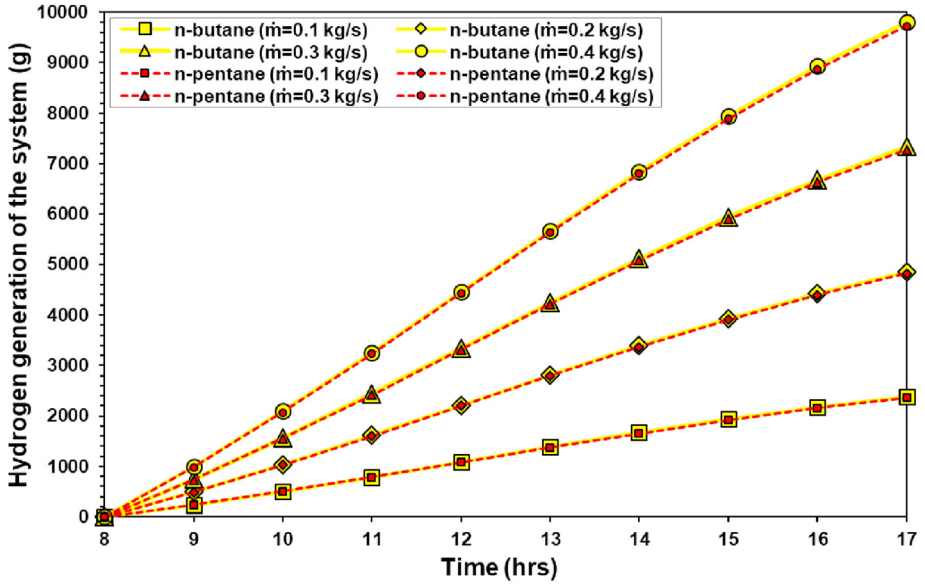

Fig. 11 – Hydrogen generation of the integrated system for the n-butane and n-pentane.

of the mass flow rate from 0.1 kg/s to 0.4 kg/s. Among the four fluids, n-butane performs the best.

As can be seen in Figs. 4–11, the efficiencies increase from morning to noon and decrease towards the evening for the working fluids the n-butane, n-pentane, and n-hexane. But severe decreases are seen in the efficiencies in the morning and evening times for the working fluid the cyclohexane.

Figs. 11 and 12 show the total daily hydrogen generation of the integrated system regarding the working fluids in the ORC. The efficiency of PEM and inverter is taken as 80% and 95% for hydrogen production.

- The daily total hydrogen is generated as 2384.6 g, 4859.2 g, 7333.6 g and 9807.1 g for the n-butane with $\dot{m} = 0.1$ kg/s, $\dot{m} = 0.2$ kg/s, $\dot{m} = 0.3$ kg/s and $\dot{m} = 0.4$ kg/s hours from 08^{00} to 17^{00}.
- The daily total hydrogen is generated as 2364 g, 4817.3 g, 7271.3 g and 9726.1 g for the n-pentane with $\dot{m} = 0.1$ kg/s, $\dot{m} = 0.2$ kg/s, $\dot{m} = 0.3$ kg/s and $\dot{m} = 0.4$ kg/s hours from 08^{00} to 17^{00}.
- The daily total hydrogen is generated as 2204.3 g, 4498.3 g, 6793 g and 9087.7 g for the n-hexane with $\dot{m} = 0.1$ kg/s, $\dot{m} = 0.2$ kg/s, $\dot{m} = 0.3$ kg/s and $\dot{m} = 0.4$ kg/s hours from 08^{00} to 17^{00}.
- The daily total hydrogen is generated as 1951.31 g, 3992.4 g, 6033.8 g and 8074.9 g for the cyclohexane with $\dot{m} = 0.1$ kg/s, $\dot{m} = 0.2$ kg/s, $\dot{m} = 0.3$ kg/s and $\dot{m} = 0.4$ kg/s hours from 08^{00} to 17^{00}.

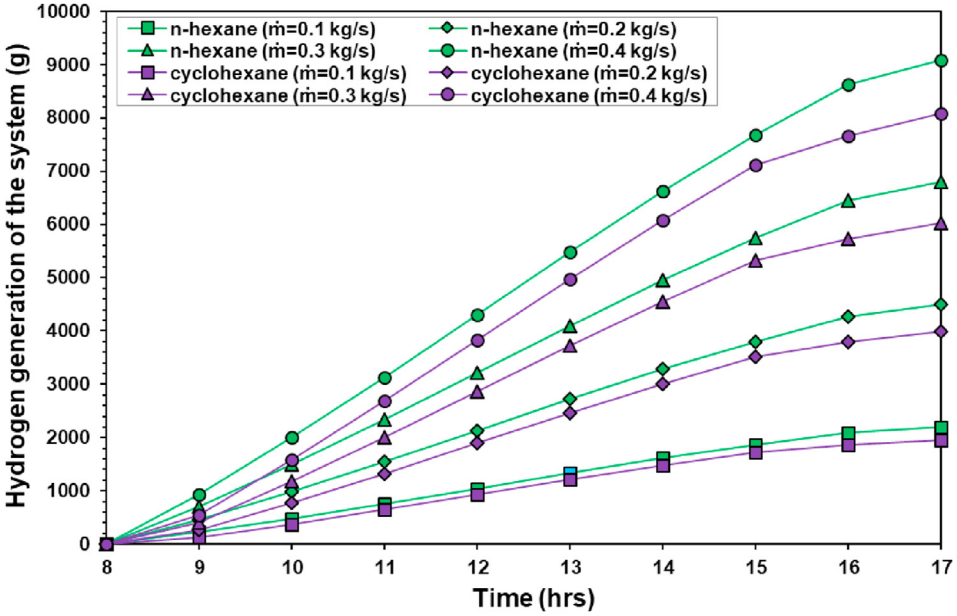

Fig. 12 – Hydrogen generation of the integrated system for the n-hexane and cyclohexane.

The highest daily hydrogen is generated for the configuration of n-butane with $\dot{m} = 0.4$ kg/s amongst 16 configurations. The lowest daily hydrogen is generated for the configuration of cyclohexane with $\dot{m} = 0.1$ kg/s.

Conclusion

In this study, the power and hydrogen production performance of an integrated renewable energy system is investigated. The system consists of PTSCs, a middle-grade geothermal source, an ORC, a PEM, and cooling towers. The thermal energy required to run the ORC can be obtained from a middle-grade geothermal source supported by the PTSCs. The temperature of the fluid of the middle-grade geothermal source can be significantly upgraded by the PTSCs that harvest solar radiation. With the integration of solar energy with geothermal source, the temperature of the fluid entering the system is increased, as well as its energy and exergy. Thus, more electricity and hydrogen are produced in the system with the fluid with high energy and exergy sent to the ORC. In addition, the best performance of the system is found by testing four types of working fluids and four different mass flow rates for each.

- The highest overall efficiency, electricity generation, and hydrogen production are obtained for the configuration of n-butane with $\dot{m} = 0.4$ kg/s between the hours of 11^{00}-13^{00}.
- The average electricity generation is 66.02 kW between the hours of 11^{00}-13^{00}.
- The system can reach up to 9807.1 g hydrogen production in a day.
- The energy and exergy efficiency is calculated to be 5.85% and 8.27% for n-butane, respectively.
- To enhance the performance of the integrated system, upgrading the temperature of the fluid of the middle-temperature geothermal source alone is not enough.
- The mass flow rate of the working fluid in the ORC should also be increased.

As a result, it is seen that the significant amount of electricity and hydrogen can be generated from a middle-grade geothermal source supported by solar energy and its energy and exergy efficiency are improved via n-butane. If the components of the integrated system are developed further, thermal energy, electricity, and hydrogen can be produced more efficiently.

Declaration of competing interest

The authors declare that they have no known competing financial interests or personal relationships that could have appeared to influence the work reported in this paper.

REFERENCES

[1] Ata R, Öcal F. Potential analysis of renewable energy sources in Manisa. C.B.U. Journal of Science 2014;10(1):1–10.

[2] Sanyal SK. Classification of geothermal systems – a possible scheme. Proceedings, thirtieth workshop on geothermal reservoir engineering, Stanford University, Stanford, California, January 31-February 2, 2005;SGP-TR-176.

[3] Li Z, Khanmohammadi S, Khanmohammadi S, Al-Rashed AAAA, Ahmadi P, Afrand M. 3-E analysis and optimization of an organic Rankine flash cycle integrated with a PEM fuel cell and geothermal energy. Int J Hydrogen Energy 2020;45:2168–85.

[4] Walraven D, Laenen B, D'haeseleer W. Minimizing the levelized cost of electricity production from low-temperature geothermal heat sources with ORCs: water or air cooled? Appl Energy 2015;142(2015):144–53.

[5] Fiaschi D, Manfrida G, Rogai E, Talluri L. Exergoeconomic analysis and comparison between ORC and Kalina cycles to exploit low and medium-high temperature heat from two different geothermal sites. Energy Convers Manag 2017;154:503–16.

[6] Yuksel YE, Ozturk M. Thermodynamic and thermoeconomic analyses of a geothermal energy based integrated system for hydrogen production. Int J Hydrogen Energy 2017;42:2530–46.

[7] Hung TC, Wang SK, Kuo CH, Pei BS, Tsai KF. A study of organic working fluids on system efficiency of an ORC using low-grade energy sources. Energy 2010;35:1403–11.

[8] Atiz A, Karakilcik H, Erden M, Karakilcik M. Investigation energy, exergy and electricity production performance of an integrated system based on a low-temperature geothermal resource and solar energy. Energy Convers Manag 2019;1951:798–809.

[9] Kalogirou SA, Karellas S, Badescu V, Braimakis K. Exergy analysis on solar thermal systems: a better understanding of their sustainability. Renew Energy 2016;85:1328–33.

[10] AlZahrani AA, Dincer I. Energy and exergy analyses of a parabolic trough solar power plant using carbon dioxide power cycle. Energy Convers Manag 2018;158:476–88.

[11] Yilmaz F, Ozturk M, Selbas R. Energy and exergy performance assessment of a novel solar-based integrated system with hydrogen production. Int J Hydrogen Energy 2019;44:18732–43.

[12] Cardemil JM, Cortés F, Díaz A. Thermodynamic evaluation of solar-geothermal hybrid power plants in northern Chile. Energy Convers Manag 2016;123:348–61.

[13] Karapekmez A, Dincer I. Thermodynamic analysis of a novel solar and geothermal based combined energy system for hydrogen production. Int J Hydrogen Energy 2020;45(919):5608–28.

[14] Wan P, Gong L, Bai Z. Thermodynamic analysis of a geothermal-solar flash-binary hybrid power generation system. Energy Procedia 2019;158:3–8.

[15] Alirahmi SM, Dabbagh SR, Ahmadi P, Wongwises S. Multi-objective design optimization of a multi-generation energy system based on geothermal and solar energy. Energy Convers Manag 2020;205:112426.

[16] Alirahmi SM, Rostami M, Farajollahi AH. Multi-criteria design optimization and thermodynamic analysis of a novel multi-generation energy system for hydrogen, cooling, heating, power, and freshwater. Int J Hydrogen Energy 2020;45(3029):15047–62.

[17] Waseem S, Ratlamwala TAH, Salman Y, Bham AA. Geothermal and solar based mutligenerational system: a comparative analysis. Int J Hydrogen Energy 2020;45:5636–52.

[18] Li K, Liu C, Jiang S, Chen Y. Review on hybrid geothermal and solar power systems. J Clean Prod 2020;25020:119481.

[19] Bonyadi N, Johnson E, Baker D. Technoeconomic and exergy analysis of a solar geothermal hybrid electric power plant using a novel combined cycle. Energy Convers Manag 2018;15615:542–54.

[20] Cao L, Lou J, Wang J, Dai Y. Exergy analysis and optimization of a combined cooling and power system driven by geothermal energy for ice-making and hydrogen production. Energy Convers Manag 2018;174:886–96.
[21] Arabhosseini A, Samimi-Akhijahani H, Motahayyer M. Increasing the energy and exergy efficiencies of a collector using porous and recycling system. Renew Energy 2019;132:308–25.
[22] Dincer I, Rosen MA. Thermodynamic aspects of renewables and sustainable development. Renew Sustain Energy Rev 2005;9:169–89.
[23] Barbier ER. Nature and technology of geothermal energy: a review. Renew Sustain Energy Rev 1997;1:1–69.
[24] Duffie JA, Beckman WA. Solar engineering of thermal process. 4th ed. New York: Wiley Interscience; 2013.
[25] Arasu AV, Sornakumar T. Design, manufacture and testing of fiberglass reinforced parabolic trough for parabolic trough solar collectors. Sol Energy 2007;81:1273–9.
[26] Petela R. Exergy of undiluted thermal radiation. Sol Energy 2003;74(6):469–88.
[27] Quoilin S, Broek MVD, Declaye S, Dewallef P, Lemort V. Techno economic survey of organic rankine cycle (ORC) systems. Renew Sustain Energy Rev 2013;22:168–86.
[28] Long R, Bao YJ, Huang XM, Lu W. Exergy analysis and working fluid selection of Organic Rankine Cycle for low grade waste heat recovery. Energy 2014;73:475–83.
[29] Cilogullari M, Erden M, Karakilcik M, Dincer I. Investigation of hydrogen production performance of a photovoltaic and thermal system. Int J Hydrogen Energy 2017;42:2547–52.
[30] Lamy C. From hydrogen production by water electrolysis to its utilization in a PEM fuel cell or in a SO fuel cell: some considerations on the energy efficiencies. Int J Hydrogen Energy 2016;41:15415–25.
[31] Hernández-Gómez Á, Ramirez V, Guilbert D. Investigation of PEM electrolyzer modeling: electrical domain, efficiency, and specific energy consumption. Int J Hydrogen Energy 2020;45:14625–39.
[32] Kumar SS, Himabindu V. Hydrogen production by PEM water electrolysis-A review. Materials Science for Energy Technologies 2019;2:442–54.